PNAS
www.pnas.org

Supplementary Information for

Rapid hydrolysis of tertiary isoprene nitrate efficiently removes NO_x from the atmosphere

K. T. Vasquez, J. D. Crounse, B. C. Schulze, K. H. Bates, A. P. Teng, L. Xu, H. M. Allen and P. O. Wennberg

Correspondence to:
P. O. Wennberg (wennberg@caltech.edu)

This PDF file includes:

Supporting Information Text

1. Caltech Field Study

Data was obtained between 01 August and 17 August 2017. During this time, the GC-CIMS instrument was located atop the central library on the Caltech campus in Pasadena, CA (44 m above ground level, 34.1368 °N, 118.126 °W). Pasadena is a part of the Los Angeles Metropolitan area and the South Coast Air Basin (SoCAB). As such, it is located near a multitude of mobile and industrial sources of anthropogenic pollution. However, the field site is also in close proximity to local vegetation which is made up of known isoprene emitters, such as oak and eucalyptus trees (1). Thus, biogenic emissions also influence the area (2, 3).

During the study, the field site experienced daytime (10:00 - 20:00 PDT) relative humidities between 42 - 64% and warm temperatures (a mean low of 20°C and a mean high of 31°C). The instrument was placed on the southwest corner of the roof of the library and inlet protruded from the south face of the building, sampling into the majority of the daytime winds. Back trajectories (Fig. S1) show that, on average, air masses passed through downtown Los Angeles approximately one hour before reaching the field site in the early afternoon.

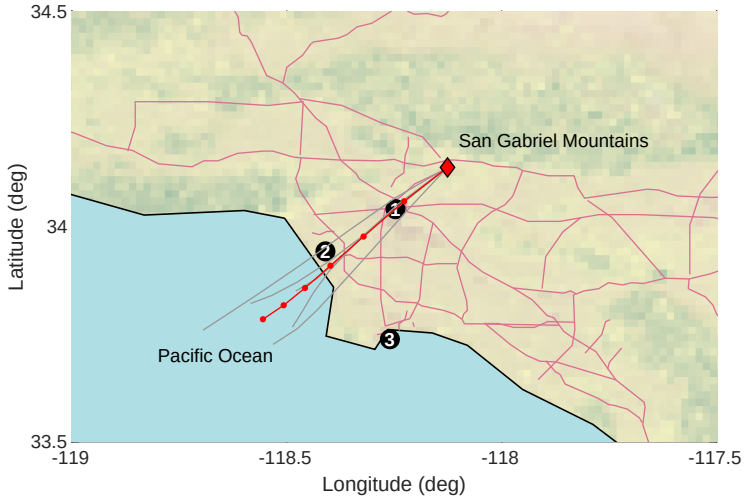

Fig. S1. Map of southern California indicating the location of the Caltech field site (red diamond), major highways (pink) and the following three locations: (1) downtown Los Angeles, (2) the Los Angeles International Airport and (3) the Port of Los Angeles. The average HYSPLIT back trajectory (4) for 15:00 PDT (red line) is shown for five randomly selected clear, sunny days during the study (gray lines). Each red circle on the average back trajectory represents 1 hour elapsed time.

2. Data Processing and Uncertainty

Data processing of the GC data presented in this work has been discussed by Vasquez et al. (5). As the 1,2-IHN and 4,3-IHN isomers are not completely separated with our GC configuration, we used a web-available MATLAB peakfit function (6) and modified it to support an exponentially modified gaussian peak shape, in which individual peaks had fixed widths and distinct tailing constants, to deconvolve the chromatogram. Peak parameters were chosen by minimizing the root mean square (rms) difference between the data and the peak fitting model. Sensitivity of the fitted peak area to the fitting parameters was estimated using a bootstrapping method (7). We varied both the chosen peak widths and tailing constants by ±40% over 1000 trials. Trials that degraded the fit beyond 1σ of the rms error were disregarded. The calculated peak areas were then scaled by their relative CIMS sensitivities and GC transmission factors, before being normalized by the volume of air collected on the column in order to determine the corresponding ambient concentrations. The CF_3O^- CIMS sensitivities of 1,2-IHN and 4,3-IHN have previously been measured to be similar (8, 9). Both isomers have been shown to have GC transmission efficiencies near 100% provided water is not condensed during the trapping period (5, 8, 9).

3. Hydrolysis Kinetics Experiments

IHN Hydrolysis in a Humid Chamber. Chamber experiments were conducted to probe the kinetics of condensed-phase hydrolysis of 1,2-IHN. For these experiments, isoprene, NO and methyl nitrite (CH_3ONO, OH source) were added to a 24 m^3 Teflon bag. UV lights were illuminated for a few minutes to oxidize approximately 10% of the isoprene in the chamber, limiting the production of second-generation products. Oxidation products were then observed in the dark using the GC-CIMS (see Materials and Methods in main text).

Experiments were performed at 50% and 85% relative humidity at 25°C (Fig. S2). During these experiments, a rapid decay of the 1,2-IHN isomer was observed and its lifetime was found to be strongly dependent on humidity levels, resulting in a

lifetime of 45 minutes at 50% RH and 15 minutes at 85% RH. In contrast, there was no observed decay of the 4,3-IHN isomer at either humidity during the course of the experiments, which is consistent with its longer lifetime against hydrolysis (10). Corresponding signal increases were observed at m/z 187 (CF_3O^- cluster with neutral of mass of 102 amu), consistent with formation of isoprene diol, a product of IHN hydrolysis. In addition, we observed an initial small production of E-1,4-IHN isomer during the dark portion of the experiments, subsequently followed by first-order decay. We hypothesize this production arises from the condensed-phase isomerization of 1,2-IHN, similar to what has been previously observed during the GC-analysis of 1,2-IHN (8).

Hydrolysis was likely occurring on the chamber walls. Similar experiments with high levels (up to 500 μg m^{-3}) of ammonium sulfate particulate mass did not alter the decay rate in a measurable manner compared to experiments without seed. Experiments conducted under dry conditions (<5% RH) had significantly lower loss rates for 1,2-IHN. Experiments conducted in a smaller chamber (1 m^3) using a clean Teflon bag showed that the 1,2-IHN concentrations remained stable at elevated humidities (>80%) over a 12 hour period, despite a higher gas-wall interaction rate. We suggest that accumulation of deposited material on the walls of the large chamber (such as H_2SO_4 and other salts derived from deposited seed particles, and possibly low-volatility organic material) can take up water under high humidity, creating a condensed-phase reservoir within which the hydrolysis can occur.

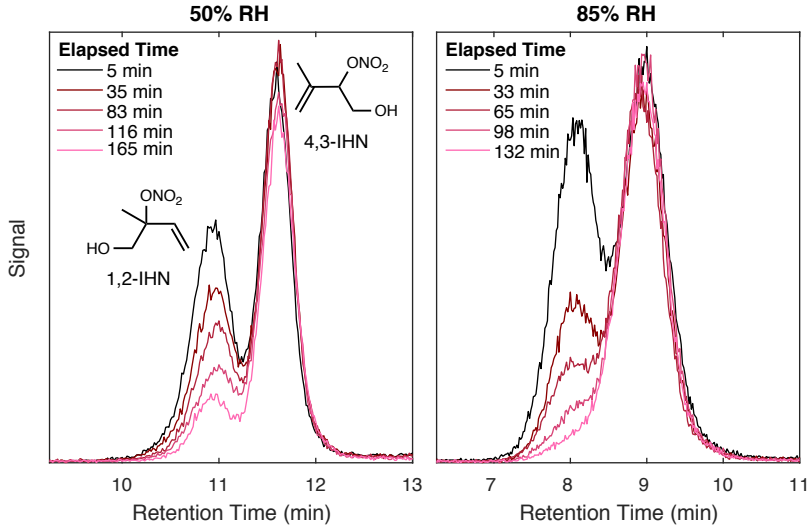

Fig. S2. High NOx isoprene oxidation experiments were performed at 50% (left) and 85% (right) RH. The lifetime of the 1,2-IHN isomers was found to be strongly dependent on humidity. Under completely dry conditions in a clean Teflon bag, the area of the 1,2-IHN isomer peak is 1.5 times that of 4,3-IHN with NO levels >500 ppbv, such that the RO_2 distribution is near the kinetic limit. We note that different temperature programs were used for these two data sets. As a result, the resolution and retention time of these isomers are not identical.

Synthesis of 1,2-IHN. 1,2-IHN synthesis was performed by combining anhydrous nitric acid with 2-methyl-2-vinyloxirane (Sigma-Aldrich) in dry dichloromethane. Special care was taken to minimize the amount of H_2O present in the reaction mixture by purging the headspace of the reaction vessel with dry nitrogen. Typical synthesis: 330 mg (4.0 mmol) 2-methyl-2-vinyloxirane was dissolved 8 ml anhydrous methylene chloride (Sigma-Aldrich). This was placed in a 100 ml round bottom flask with a teflon-coated magnetic stir bar, briefly purged with dry N_2, and cooled to -10°C using an isopropanol bath that was cooled with liquid nitrogen. With rapid stirring, a mixture of 250 mg (4.0 mmol) anhydrous HNO_3 in 7 ml methylene chloride was slowly added (1-2 drops per second) with N_2 purge. After HNO_3 addition, the cold bath was removed, and the mixture was allowed to warm to room temperature with stirring. Anhydrous HNO_3 was produced just before each synthesis using the reaction of $NaNO_3$ with H_2SO_4, as described by McCabe, et al. (11). Products were analyzed by evaporating a small amount of the crude reaction mixture into a 100 L Teflon pillow bag and analyzing the gas composition with the GC-CIMS. Initially, 1,2-IHN was the most abundant IHN isomer (1,2-IHN >70% of total IHN). Using gas-phase quantification (GC-CIMS), total IHN yield was small (typically a few percent (mol/mol) of the starting epoxide). Separation of 1,2-IHN from other products in the reaction mixture was attempted using flash chromatography with silica gel, however, no 1,2-IHN was collected from the column. It is likely that residual H_2O or hydroxy groups attached directly to the silica gel is sufficient to hydrolyze the 1,2-IHN on the column.

^{1}H NMR spectra of the crude reaction mixture (after removal of the methylene chloride by vacuum distillation at -15°C) is shown in Fig. S3. Signals arising from 1,2-IHN are identified by comparing the initial NMR spectra to one taken after leaving the reaction mixture at room temperature for 4 hours and observing which signals decayed (Fig. S4). 1,2-IHN is highly reactive. We observe that 1,2-IHN (crude reaction mixture) decays in dry methylene chloride at -15° C with a lifetime of ~1 day, likely through reactions with itself, or other species present in the reaction mixture.

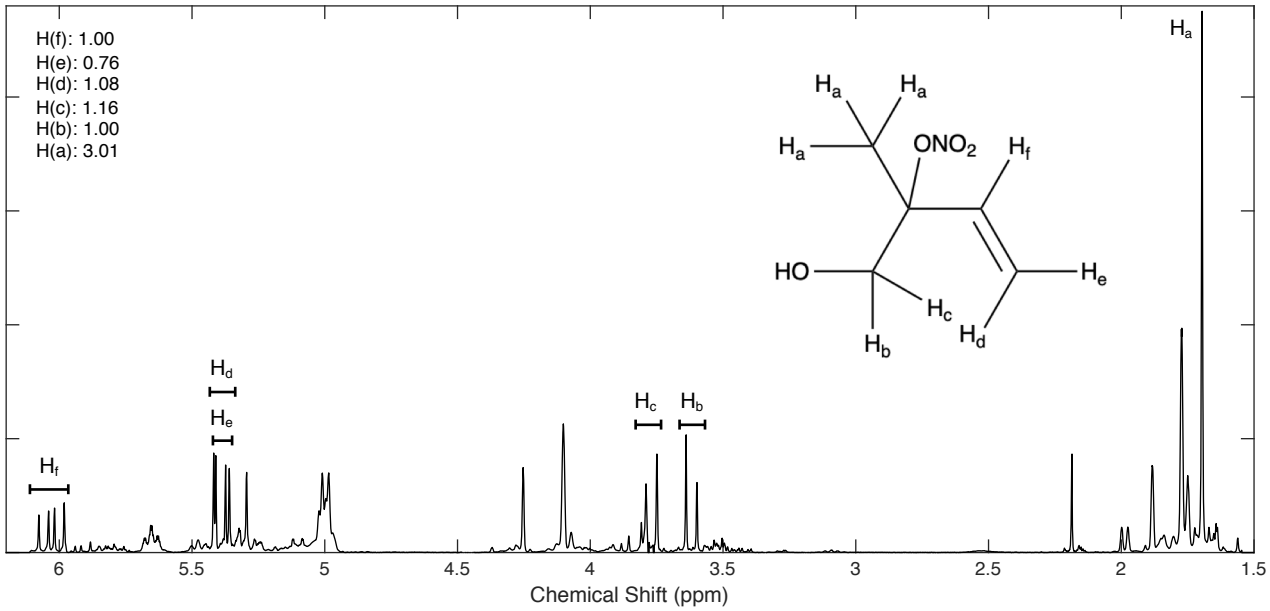

Fig. S3. ^{1}H NMR spectra (300 MHz) of 1,2-IHN in deuterated chloroform (Sigma Aldrich, 99.8% D). δ 6.03 (dd, J = 17.7, 11.0 Hz, 1H-H_f), 5.394 (d, J = 11.0, Hz, 1H-H_e), 5.391 (d, J = 17.6, Hz, 1H-H_d), 3.77 (d, J = 12.2, Hz, 1H-H_c), 3.62 (d, J = 12.3, Hz, 1H-H_b), 1.70 (s, 3H-H_a). It appears that the geminal coupling between H_d and H_e is quite small and not resolved with this spectrometer.

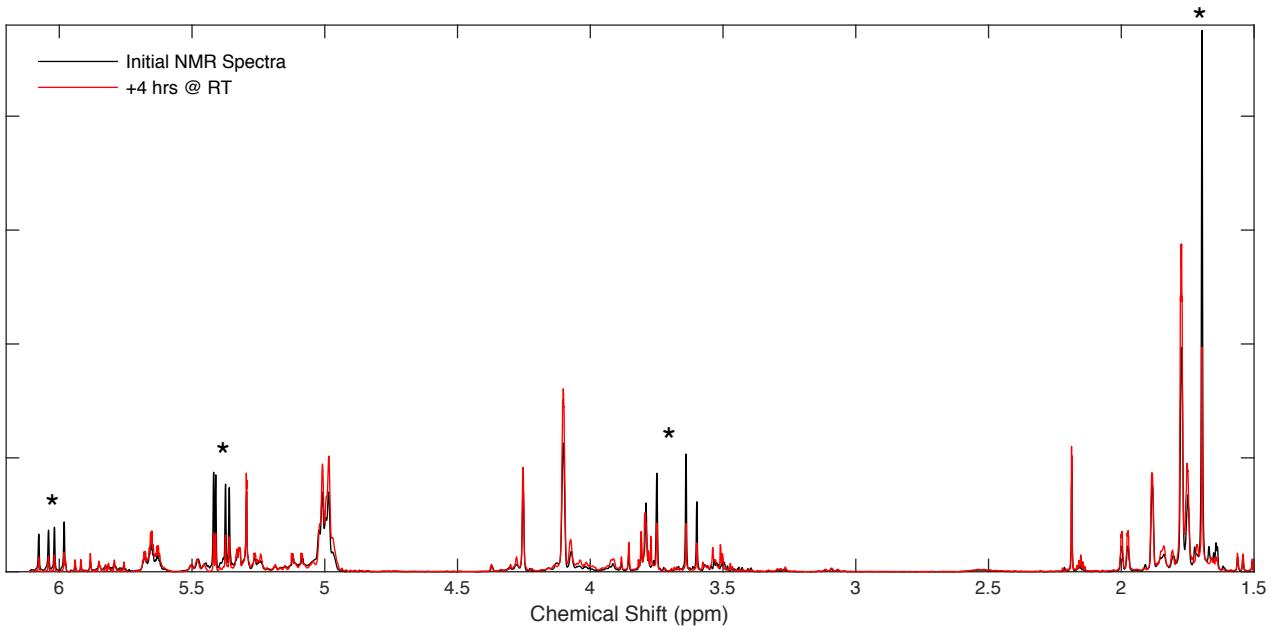

Fig. S4. ^{1}H NMR spectra of crude 1,2-IHN synthetic mixture taken 4 hours apart with sample resting at room temperature between analyses. Signals strongly decaying with time are believed to arise from 1,2-IHN hydrogens (*).

Synthesis of 4,3-IHN. Synthesis of 4,3-IHN was conducted in a manner similar to the IHN synthesis described by Lee et al. (9) In place of 2-methyl-2-vinyloxirane, (1-methylethenyl)oxirane was used. Because this epoxide is not commercially available it was synthesized according to the method described by Harwood, et al.,(12) though scale was reduced by factor of 4. After synthesis of the hydroxy nitrate, the crude reaction mixture was analyzed using GC-CIMS as described above for 1,2-IHN. The distribution of the IHN isomers as analyzed in the gas-phase was: 89% 4,3-, 1% Z-4,1-, and 10% E-4,1-IHN. The overall IHN molar yield was approximately 13% of the starting epoxide. After removal of methylene chloride at -15°C using vacuum, the

crude mixture was purified using flash chromatography. A column composed of six inches of 400 mesh silica gel within a 2.54 cm O.D. pyrex tube was prepared using a solvent mixture of 1:1 ethyl acetate:hexanes. After flowing about 1 column volume of solvent to condition the column, the concentrated crude reaction mixture was charged to the top of the column. The column was run under gravity for about 4 hours, collecting 5-15 ml aliquots, monitoring the output composition using TLC, and CIMS. A C_5-diol was found to elute very rapidly (first 2-3 aliquots). The IHN isomers eluted much later, however, separation of the isomers was quite good when collecting 5 ml aliquots. Elution order was observed to be 4,3-, *Z*-4,1-, *E*-4,1-IHN, as verified by NMR and GC-CIMS. Aliquots containing the same isomers were combined, solvent was removed, and products were diluted with methylene chloride for storage.

IHN Hydrolysis in D_2O. IHN hydrolysis kinetics in D_2O were studied using ^1H NMR methods similar to experiments described by Eddingsaas et al. (13). NMR spectra were acquired using a Varian 600 MHz spectrometer with sample probe controlled to 25° C. Additional reference spectra were collected in $CDCl_3$ using a Varian 300 MHz instrument. For the kinetics experiments, an NMR tube was charged with D_2O and used to tune the spectrometer, collecting a single sample. The tube was then removed from the NMR and a small aliquot of the 1,2-IHN concentrated synthetic mixture was combined with the D_2O in the NMR tube. The tube was inverted several times to promote mixing, and quickly reinserted into the NMR probe. Sequential spectra were collected over time with an acquisition period of 22.6 s. A period of approximately 45 s elapsed between addition of the synthetic mixture to the D_2O and the end of acquisition for the first spectrum. While signals from 1,2-IHN, *E* and *Z*-1,4-IHN are readily apparent in reference spectra in $CDCl_3$, no signals from 1,2-IHN are observed for spectra in D_2O.

As no 1,2-IHN signals were observed in the NMR spectra of the D_2O sample, we can only place lower limits on the hydrolysis rate of 1,2-IHN in D_2O at 298 K. Using the signal to noise of the NMR spectra in D_2O experiment, signals from the *E* and *Z*-1,4-IHN in the D_2O experiment, the ratio of signals from 1,2-IHN to *E*- or *Z*-1,4-IHN, and assuming the initial distribution of isomers is the same between the reference and the D_2O experiments, we constrain the hydrolysis lifetime of 1,2-IHN in D_2O to be less than 10 s.

The hydrolysis rate coefficients of *E* and *Z*-1,4-IHN in D_2O at 298 K were measured to be $(10.1 \pm 0.4) \times 10^{-3}$ s^{-1} and $(5.3 \pm 0.2) \times 10^{-3}$ s^{-1}, respectively (Fig. S5). The bulk hydrolysis rate of *E* and *Z*-1,4-IHN has been previously reported by Jacobs et al. (10) as $(6.76 \pm 0.09) \times 10^{-3}$ s^{-1}. At the time, Jacobs et al. (10) could not resolve these two isomers. Subsequently, in $CDCl_3$ they determined that the mixture had a ratio of 2.6:1 (14). Using this initial ratio and the isomer specific rate constants to calculate the total 1,4-IHN amount over the time scale of the Jacob et al. (10) experiments, these two studies are in broad agreement.

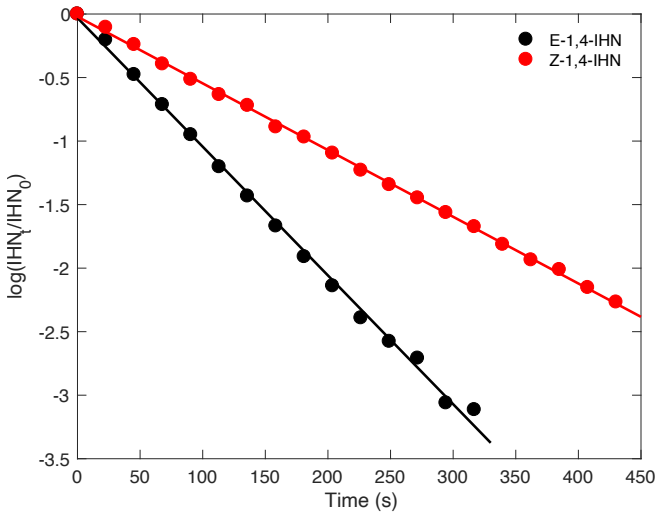

Fig. S5. First-order decay of NMR signal for *E*-1,4-IHN (black) and *Z*-1,4-IHN (red) in D_2O at 298 K.

4,3-IHN Henry's Law Constants. A known volume of the 4,3-IHN solution was combined with 6 mL H_2O in a multi-neck round bottom flask (RBF). The flask was cooled to 0°C in an ice bath with stir bars in both the RBF and the ice bath, slowly stirring. A small flow of N_2 was passed through the headspace of the RBF using a flow controller. After the RBF, a large flow of N_2 diluted the effluent from the RBF and carried the analytes to the CIMS where the 4,3-IHN was quantified. Using the ratio of the gas flows, the concentration above the solution was calculated. This, along with the assumption of headspace saturation (which was checked by reducing the flow though the RBF by a factor of 2), allowed for calculation of the Henry's Law constant. Similar methods were used to quantify the Henry's law constant of 4,3-IHN in octanol. The results from these experiments are listed in Table S1. It was not possible to determine the Henry's law constant for 1,2-IHN in water or octanol using this method.

Table S1. Experimentally determined Henry's law constants (K_H) for 4,3-IHN in water and octanol at 0°C

	K_H (10^4 M atm^{-1})	
Isomer	Water	Octanol
4,3-IHN	3.1 ± 0.8	0.9 ± 0.3

4. IHN Photolysis

To estimate the photolysis rate, a 1 m^3 Teflon bag containing synthesized 1,2-IHN was placed in direct sunlight for five hours in Pasadena, CA on March 26, 2015 between 10:00 –15:00 local time. 50 μL of the 1,2-IHN reaction mixture was combined with 650 μL acetone and a droplet of this solution was placed in a three-way vial. Dry air was then blown over this droplet, and the evaporated reaction mixture was collected in a FEP Teflon pillow bag. Contents of the bag were measured with the GC-CIMS both before and after exposure to sunlight. Chromatograms show that 1,2-IHN, and *E* and *Z*-1,4-IHN were present in significant quantities and 4,3-IHN was present in trace amounts. 1,2-butanediol was added to the bag to estimate OH oxidation during the experiment. It is assumed that 1,2-butanediol did not photolyze significantly over the time scale of this experiment.

Over the course of five hours of exposure to sunlight, after correcting for OH oxidation (using butanediol signal), 1,2-IHN decreased by about 10%. This places an upper limit to the photolysis rate of $(1.0 \pm 1.0) \times 10^{-5}$ s^{-1} for this experiment. Adjusting this number for the difference in photon flux between March 26 and August 1, we calculate an upper limit to the 1,2-IHN photolysis rate of 1.2×10^{-5} s^{-1} or approximately 22 daylight hours.

5. 1D Model Description

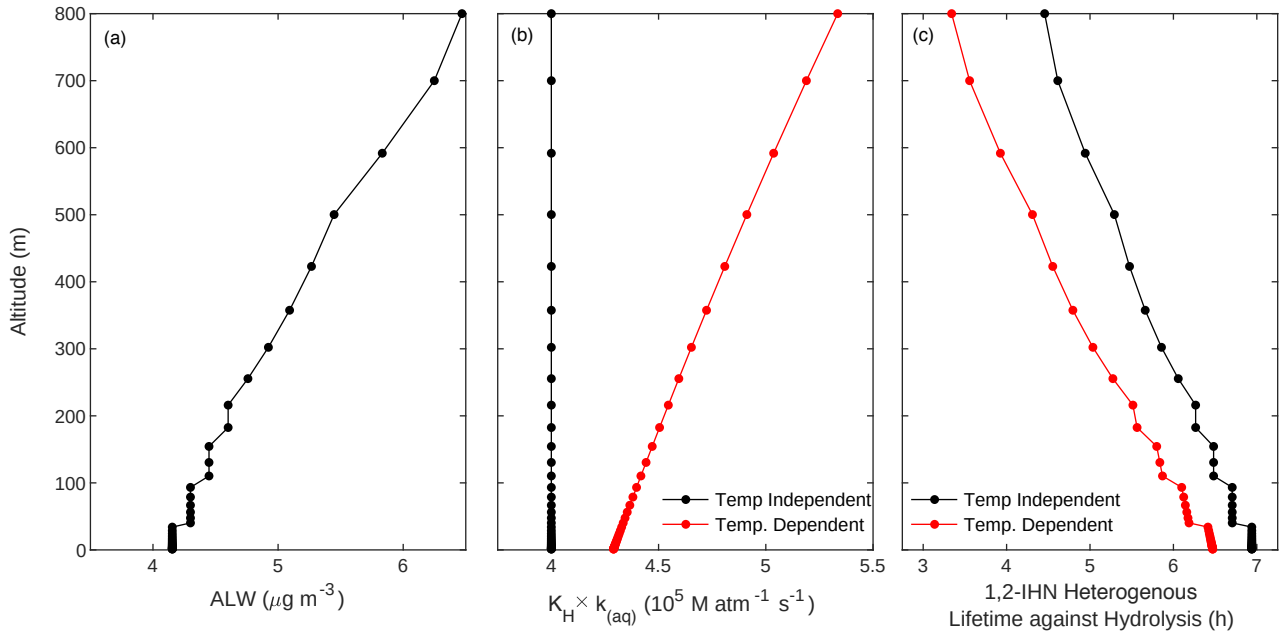

Fig. S6. Midday (noon local time) Los Angeles boundary layer profile of (a) the calculated aerosol liquid water (ALW) used to model IHN partitioning, (b) the product of the estimated 1,2-IHN Henry's law constant (K_H) and aqueous hydrolysis rate ($k_{(aq)}$) using both temperature independent (black) and dependent (red) values, and (c) the 1,2-IHN heterogenous lifetime against hydrolysis calculated from our model using temperature independent (black) and dependent (red) values of K_H and $k_{(aq)}$.

The one-dimensional (1D) atmospheric model used in this work simulates the emission, deposition, vertical transport, and photochemical oxidation of 250 chemical species in an atmospheric column tuned to replicate conditions observed during the 2010 CalNex campaign (May–June, 2010). The model consists of 40 vertical layers ranging from the ground (0.05 m) to 800 m. The first 39 layers exist within the range of the daytime boundary layer, with the 40th layer representing the free troposphere. Depending on the time of day, the uppermost layers (33–40) represent either the boundary layer or the nocturnal residual layer. Layer heights within the boundary layer are calculated similarly to previous 1D models and increase exponentially with altitude (15, 16), while the free troposphere layer has a prescribed depth of 100 m. Simulations are run for 24 hours with a time step of one minute. Diurnal meteorological variables and emission rates are provided as model inputs, as explained in more detail subsequently.

Vertical transport is simulated in the model using K-theory, a first-order flux-gradient approach common to 1D atmospheric models (15–17). Layer-specific K-values, or eddy diffusivities, are calculated using the following equation (16):

$$K_i = l_i^2 \left| \frac{dv}{dz_i} \right| f \quad [1]$$

where l_i is the vertical length scale for eddies in each layer, $\frac{dv}{dz_i}$ is the local vertical gradient of horizontal wind velocity, and f represents a stability parameter. From 10:00–17:00, the boundary layer is assumed to be fully developed and K-values are calculated from the ground to 700 m using vertical wind profiles calculated from ground level measurements. At night (20:00–06:00), mixing is effectively restricted to the bottom 250 m, meant to represent the nocturnal boundary layer in the Los Angeles area. During development and decline of the boundary layer (06:00–10:00 and 17:00–20:00), K-values are interpolated between those used at night and midday. Midday mixing between the top of the boundary layer and the free troposphere is assigned a K-value of 5 m^2 s^{-1}. Simulated IHN isomer ratios are insensitive to the free tropospheric layer depth and the mixing rate between the boundary layer and the free troposphere.

The model combines the RACM2 chemical mechanism (18), which simulates oxidation of lumped VOC classes for use in regional models, with the condensed isoprene oxidation mechanism from Wennberg et al. (19), resulting in a system with 250 chemical species and 583 chemical reactions. Photolysis rates provided by the individual mechanisms are scaled to achieve agreement between modeled and measured values of the hydroxyl radical during CalNex 2010 (20) and the photolysis rate of NO_2 (jNO_2). Emissions of non-biogenic lumped VOCs used in the RACM2 mechanism were obtained from the California Air Resources Board (CARB) database. Emissions data were available for the week of July 22–28, 2012. While these data do not correspond with the exact timeframe of the CalNex campaign, the use of data from Juneand the inclusion of an advective term described below produce reasonable simulation of the lumped VOC concentrations and there is good agreement between measured and modeled oxidant concentrations. Given uncertainty in local isoprene emissions due to vegetation heterogeneity in and around the Pasadena area, we performed sensitivity tests to determine a reasonable peak emission rate that, when diurnally scaled by the solar zenith angle, produced agreement between measured and modeled isoprene concentrations. This process suggests a peak effective rate of ~0.3 mg m^2 hr^{-1}. This value agrees well with model estimates for the region using the MEGAN model (21, 22).

Two types of advective processes are simulated within the model. Given the difficulty in quantifying the influence of advection on local concentrations, we include an advective mixing term similarly to Wolfe and Thornton (15) that pushes the model towards agreement with measured diurnal concentrations. The magnitude of this first order advective term is proportional to the difference between the modeled and measured concentration at each step. This advective term is only incorporated for parent VOCs, NO, NO_2, and O_3 in the bottom 20 layers of the model, which encompasses the region from the ground to ~20 m. Importantly, this term is not included in the differential equations governing IHN isomer production and loss. The model also includes an advective loss term to prevent unrealistic accumulation of oxidation products within the column. The magnitude of this loss rate is based on layer-dependent horizontal wind velocities and an assumed width of the Los Angeles basin ($k_{wind} = v_i/125$ km) (23).

Deposition velocities of IHN isomers are assumed to follow a diurnal pattern proportional to the cosine of the solar zenith angle with peak (midday) value of 2 cm s^{-1}, following measurements by Nguyen et al. (24). Deposition velocities of other species are calculated using the formula of Gao et al. (25) for deposition to the ground, with Henry's law constants and reactivity values taken from Ashworth et al. (17). The model assumes deposition occurs within the lowest 5 m of the domain, and first-order deposition rates are calculated by dividing the deposition velocity by this 5 m sub-domain height (23).

Diurnal mass loadings of aerosol liquid water (ALW) used to model IHN partitioning were calculated using ISORROPIA-II (26). Ground-level measurements of temperature, relative humidity, and mass loadings of inorganic aerosol components (SO_4, NH_4, and NO_3) collected during CalNex 2010 were used as model inputs. The CalNex data set for the LA ground site is publicly available at https://esrl.noaa.gov/csl/groups/csl7/measurements/2010calnex/Ground/DataDownload. Organic aerosol was not assumed to contribute to water uptake. Other salts not accurately quantified (e.g., Cl, Na, etc) were not included in the ALW calculation given their small contribution to aerosol mass loadings in the Los Angeles region (27). Aerosol mass loadings were assumed constant with altitude. The assumption of vertically invariant aerosol mass loadings is likely inaccurate in the early morning, as vehicular emissions within a shallow boundary layer produce substantial inorganic nitrate aerosol (27), increasing ALW in the boundary layer but not the residual layer. However, without additional constraints or more complex modeling it is difficult to quantify the influence of this assumption. Nevertheless, assuming a constant aerosol vertical profile should lead to an overestimate of the integrated amount of ALW within the column, rather than an underestimate, therefore producing a conservative (i.e., low) estimate of the IHN $K_H \times k_{(aq)}$ product (k^*_{hydro}).

Both Henry's law coefficients (K_H) as well as the aqueous hydrolysis rate ($k_{(aq)}$) are functions of temperature. Unfortunately, these dependences are not well-known for the IHN isomers, therefore we provide the following estimates for these parameters:

$$K_H(T) = K_H(273)\frac{e^{9622/T}}{e^{9622/273}} \quad [2]$$

$$k_{(aq)}(T) = k_{(aq)}(298K)\frac{e^{-6000/T}}{e^{-6000/298}} \quad [3]$$

The temperature dependence for K_H is based on findings from Shepson et al. (28). $k_{(aq)}$ simply assumes a doubling in the hydrolysis rate for every 10 degrees increase in temperature. For 4,3-IHN, $k_{(aq)}$(298 K) is taken from Jacobs et al. (10) as

1×10^{-5} s^{-1}. For 1,2-IHN, we only constrain k^*_{hydro}, the product of $k_{(aq)}$ and K_H. While the temperature dependences of $k_{(aq)}$ and K_H are both large, they have opposite signs, and thus in the product, k^*_{hydro}, they largely cancel, increasing by only a factor of 1.25 from the ground to the top of the boundary layer for midday simulations (Fig. S6).

While we do not know the K_H for 1,2-IHN in water, we can estimate a likely range. The lower limit is likely the K_H of 4,3-IHN, as polar functionalities near the methyl group will increase solvation in water. For example, Henry's law constant for 1,2-ISOPOOH is approximately an order of magnitude larger than 4,3-ISOPOOH (29). For the upper limit, we suggest the K_H of 4,3-IHN scaled by the ratio of the K_H for 1,2-ISOPOOH to 4,3-ISOPOOH. We hypothesize that due to hydrogen bonding, the hydroperoxide functionality acts as a better solvating group than the nitrate group, thus the difference for the solubility of the hydroperoxides in water will be larger than for the nitrates. Together, we estimate a range of K_H for 1,2-IHN of $3.1 \times 10^4 - 3.1 \times 10^5$ M atm^{-1} at 273 K, or $1.6 \times 10^3 - 1.6 \times 10^4$ M atm^{-1} at 298 K. From this range in K_H, along with our constraint for k^*_{hydro} (main text), the range in hydrolysis rate, $k_{(aq)}$, for 1,2-IHN is likely between 25 and 250 s^{-1} at 298 K. While this implies a very fast hydrolysis rate for 1,2-IHN, it is not inconsistent with our observations.

Between the CalNex-LA observations and 2017 when these measurements were made, NO_x levels declined. We have performed sensitivity studies and find the best fit to the atmospheric data (Fig. 3, main text) is not significantly impacted by the NO_x reductions.

6. GEOS-Chem

Description of GEOS-Chem Simulations. Simulations of 1,2-IHN hydrolysis and its effects were conducted using version 11-02c of the GEOS-Chem global chemical transport model (30), run at $2^\circ \times 2.5^\circ$ horizontal resolution with 72 vertical layers extending through the stratosphere. GEOS-Chem incorporates assimilated meteorological observations from the NASA Goddard Earth Observing System - Forward Processing (GEOS-FP) data product from the NASA Global Modeling and Assimilation Office (GMAO). We used the standard HEMCO emissions (31), including isoprene emissions from the MEGAN v2.1 inventory scaled uniformly to 535 Tg a^{-1} (21), along with observationally fixed tropospheric methane. We conducted both month-long (1 - 31 July 2014) and annual (1 August 2014 - 31 July 2015) simulations, following one year of initialization from 1 July 2013.

GEOS-Chem incorporates an editable chemical mechanism with gas-phase and heterogeneous chemistry. For all simulations performed herein, we replaced the default isoprene oxidation scheme with the Mini-CIM mechanism described in Bates et al. (32), which separates the 1,2- and 4,3-IHN isomers and incorporates a number of additional updates to isoprene chemistry based on the reduced mechanism compiled by Wennberg et al. (19). The aerosol uptake and hydrolysis of isoprene nitrates in GEOS-Chem is parameterized with an irreversible reactive uptake coefficient (γ) onto the aqueous inorganic component of aerosol. In their analysis of organic nitrate chemistry in the Southeast United States, Fisher et al. (33) used a constant γ of 0.005 for all isoprene nitrates. Marais et al. (34) introduced a mechanistic formulation for γ based on an effective overall hydrolysis rate, k^*_{hydro} (M atm^{-1} s^{-1}), which incorporates an effective Henry's law constant (K_H, M atm^{-1}), accounting for rapid dissociation or hydration equilibria in the aqueous phase) and a pseudo-first-order aqueous-phase reaction rate constant ($k_{(aq)}$, s^{-1}). Marais et al. (34) used $K_H = 3.3 \times 10^5$ M atm^{-1} for all isoprene-derived nitrates, $k_{(aq)} = 1.6 \times 10^{-5}$ s^{-1} for lumped β-hydroxynitrates, and $k_{(aq)} = 6.8 \times 10^{-3}$ s^{-1} for δ-hydroxynitrates and dihydroxy-dinitrates. Here, we updated the K_H of 4,3-IHN to match the value listed in Table S1, and reduce its $k_{(aq)}$ to 1×10^{-5} s^{-1}. For 1,2-IHN, we perform individual simulations with k^*_{hydro} values of 0, 3×10^4, 3×10^5, 3×10^6, and 3×10^7 M atm^{-1} s^{-1}, all invariant with temperature. In our analysis, we compared the resulting mixing ratios as well as total production and loss of species of interest between these simulations employing different 1,2-IHN k^*_{hydro} values and against simulations using the baseline uptake parameterizations from Marais et al. (34) and Fisher et al. (33). We acknowledge that there is an inconsistency in the modeling of the 4,3-IHN hydrolysis loss and the experimental determinations of this quantity. The 273 K value for K_H is used in GEOS-Chem along with the 298 K value for $k_{(aq)}$. Using the temperature dependencies above leads to a hydrolysis rate for the 4,3-IHN that is about 6 times too fast. We note, however, that this does not impact our results, as even using the faster hydrolysis rate, 4,3-IHN hydrolysis is negligible compared to the overall loss rate.

We also include the hydrolysis of monoterpene nitrates (MTN), as implemented in the current default GEOS-Chem set up. As currently described in Fisher et al. (33), this chemistry is largely based on the scheme developed by Browne et al. (35) for use in WRF-Chem, which was built on the RACM2 scheme developed by Goliff et al. (18). GEOS-Chem assumes a bulk lifetime of monoterpene nitrates against hydrolysis of 1 h (33), which was found to simulate measured particle organic nitrate mass during the SOAS and SEAC^{4}RS campaigns better than the longer lifetimes estimated in field and laboratory analyses (36–38). However, this hydrolysis lifetime is poorly constrained and is rendered particularly uncertain by the many simplifying assumptions underlying the GEOS-Chem MTN parameterization, including the lumping of the parent monoterpenes into two representative precursor species, their heavily abridged oxidation mechanism, the lumping of MTN into two representative species (those with and without double bonds), and the fixed reactive uptake coefficient of $\gamma = 0.01$ for all MTN. In light of the changes we make in this work to the budget of organic nitrates, the MTN parameterization in GEOS-Chem should be reassessed.

Lastly, in our simulations, we do not include fast tertiary nitrate hydrolysis of the other compounds besides IHN. Thus, these simulations may underestimate the contribution of hydrolysis towards shortening the NO_x lifetime. As one example, OH oxidation of 1,2-isoprene hydroperoxy nitrate (IPN) is thought to yield several second-generation tertiary nitrates (19), which will also likely undergo rapid hydrolysis.

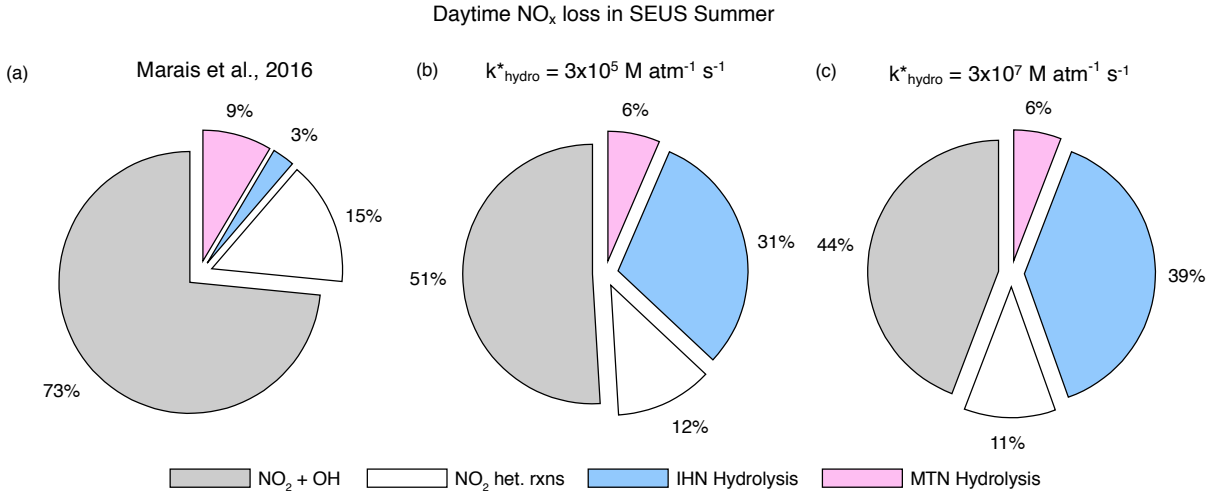

Fig. S7. Pie charts showing the global impact IHN hydrolysis has on the different daytime NO_x pathways in the lower 1 km of the atmosphere over the southeast USA in the summer when (a) using parameters from Marais et al. (34), (b) setting k^*_{hydro} to 3×10^5 M atm^{-1} s^{-1}, and (c) setting k^*_{hydro} to 3×10^7 M atm^{-1} s^{-1}. The global impact of this chemistry remains largely unchanged when $k^*_{\mathrm{hydro}} > 3 \times 10^5$ M atm^{-1} s^{-1}.

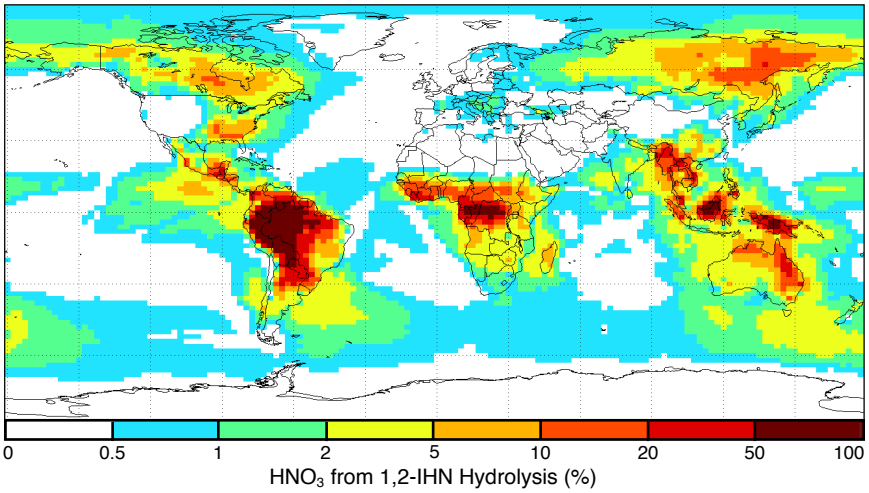

Fig. S8. Annually averaged fraction of HNO_3 attributed to 1,2-IHN hydrolysis in the lowest 1 km of the atmosphere, as calculated with GEOS-Chem when a 1,2-IHN hydrolysis rate of $k^*_{\mathrm{hydro}} = 3 \times 10^5$ M atm^{-1} s^{-1} has been included.

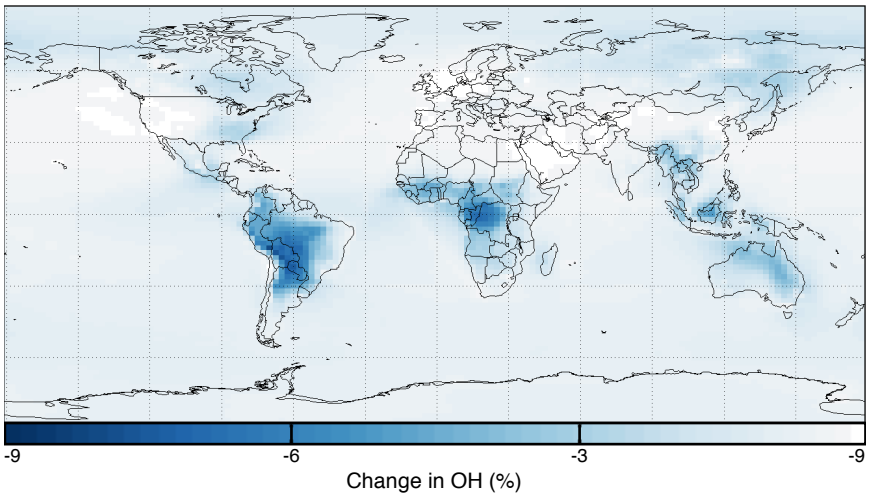

Fig. S9. Annually averaged change in OH in the lowest 1 km of the atmosphere when comparing the standard GEOS-Chem model with one that includes a 1,2-IHN hydrolysis rate of $k^*_{\mathrm{hydro}} = 3 \times 10^5$ M atm^{-1} s^{-1}.

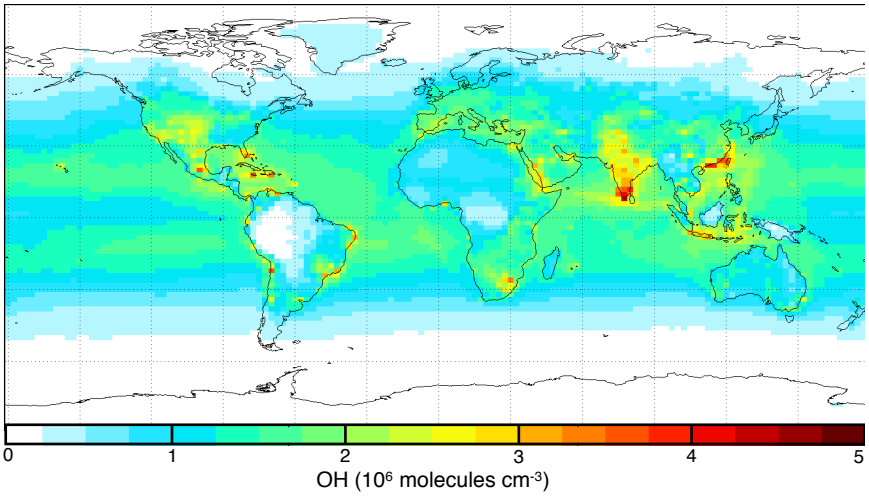

Fig. S10. Annually averaged OH concentrations in the lowest 1 km of the atmosphere, as calculated with GEOS-Chem when a 1,2-IHN hydrolysis rate of $k^*_{\mathrm{hydro}} = 3 \times 10^5$ M atm^{-1} s^{-1} has been included.

References

1. Guenther A, Zimmerman P, Wildermuth M (1994) Natural volatile organic compound emission rate estimates for U.S. woodland landscapes. *Atmos. Environ.* 28(6):1197 – 1210.
2. Washenfelder RA, et al. (2011) The glyoxal budget and its contribution to organic aerosol for Los Angeles, California, during CalNex 2010. *J. Geophys. Res.-Atmos.* 116(D21).
3. Pollack IB, et al. (2013) Trends in ozone, its precursors, and related secondary oxidation products in Los Angeles, California: A synthesis of measurements from 1960 to 2010. *J. Geophys. Res.-Atmos.* 118(11):5893–5911.
4. Stein AF, et al. (2015) NOAA's HYSPLIT atmospheric transport and dispersion modeling system. *Bull. Amer. Meteor. Soc.* 96(12):2059 – 2077.
5. Vasquez KT, et al. (2018) Low-pressure gas chromatography with chemical ionization mass spectrometry for quantification of multifunctional organic compounds in the atmosphere. *Atmos. Meas. Tech.* 11:6815 – 6832.
6. O'Haver T (2017) Peak fitters (https://terpconnect.umd.edu/~toh/spectrum/InteractivePeakFitter.htm). Accessed 30 June 2018.
7. Praske E, et al. (2018) Atmospheric autoxidation is increasingly important in urban and suburban North America. *P. Natl. Acad. Sci.* 115(1):64 – 69.
8. Teng AP, Crounse JD, Wennberg PO (2017) Isoprene peroxy radical dynamics. *J. Am. Chem. Soc.* 139(15):5367 – 5377.
9. Lee L, Teng AP, Wennberg PO, Crounse JD, Cohen RC (2014) On rates and mechanism of OH and O_3 reactions with isoprene-derived hydroxy nitrates. *J. Phys. Chem. A* 118(9):1622 – 1637.
10. Jacobs MI, Burke WJ, Elrod MJ (2014) Kinetics of the reactions of isoprene-derived hydroxynitrates: Gas phase epoxide formation and solution phase hydrolysis. *Atmos. Chem. Phys.* 14(17):8933 – 8946.
11. McCabe DC, et al. (2003) Kinetics of the removal of OH(v=1) and OD(v=1) by HNO_3 and DNO_3 from 253 to 383 K. *J. Phys. Chem. A* 107(39):7762–7769.
12. Harwood LM, Casey G, Sherlock J (1990) A simple laboratory procedure for preparation of (1-methylethenyl)oxirane (3,4-epoxyisoprene). *Synth. Chem.* 20(9):1287–1292.
13. Eddingsaas NC, VanderVelde DG, Wennberg PO (2010) Kinetics and products of the acid-catalyzed ring-opening of atmospherically relevant butyl epoxy alcohols. *J. Phys. Chem. A* 114(31):8106–8113.
14. Elrod M (2020) personal communication.
15. Wolfe GM, Thornton JA (2011) The Chemistry of Atmosphere-Forest Exchange (CAFE) model, part 1: Model description and characterization. *Atmos. Chem. Phys.* 11(1):77 – 101.
16. Bryan AM, et al. (2012) In-canopy gas-phase chemistry during CABINEX 2009: Sensitivity of a 1-D canopy model to vertical mixing and isoprene chemistry. *Atmos. Chem. Phys.* 12(18):8829 – 8849.
17. Ashworth K, et al. (2015) FORest Canopy Atmosphere Transfer (FORCAsT) 1.0: A 1-D model of biosphere-atmosphere chemical exchange. *Geosci. Model Dev.* 8(11):3765 – 3784.
18. Goliff WS, Stockwell WR, Lawson CV (2013) The regional atmospheric chemistry mechanism, version 2. *Atmos. Environ.* 68:174 – 185.
19. Wennberg PO, et al. (2018) Gas-phase reactions of isoprene and its major oxidation products. *Chem. Rev.*
20. Griffith SM, et al. (2016) Measurements of hydroxyl and hydroperoxy radicals during CalNex-LA: Model comparisons and radical budgets. *J. Geophys. Res.-Atmos.* 121(8):4211 – 4232.
21. Guenther AB, et al. (2012) The Model of Emissions of Gases and Aerosols from Nature version 2.1 (MEGAN2.1): An extended and updated framework for modeling biogenic emissions. *Geosci. Model Dev.* 5(6):1471 – 1492.
22. Misztal PK, et al. (2016) Evaluation of regional isoprene emission factors and modeled fluxes in California. *Atmos. Chem. Phys.* 16(15):9611 – 9628.
23. Pratt KA, et al. (2012) Contributions of individual reactive biogenic volatile organic compounds to organic nitrates above a mixed forest. *Atmos. Chem. Phys.* 12(21):10125 – 10143.
24. Nguyen TB, et al. (2015) Rapid deposition of oxidized biogenic compounds to a temperate forest. *P. Natl. Acad. Sci.* 112(5):E392 – E401.
25. Gao W, Wesely ML, Doskey PV (1993) Numerical modeling of the turbulent diffusion and chemistry of NOx , O_3, isoprene, and other reactive trace gases in and above a forest canopy. *J. Geophys. Res.-Atmos.* 98(D10):18339 – 18353.
26. Fountoukis C, Nenes A (2007) ISORROPIA II: A computationally efficient thermodynamic equilibrium model for K^+-Ca^{2+}-Mg^{2+}-NH_4^+-Na^+-SO_4^{2-}-NO_3^--Cl^--H_2O aerosols. *Atmos. Chem. Phys.* 7(17):4639 – 4659.
27. Hayes PL, et al. (2013) Organic aerosol composition and sources in Pasadena, California, during the 2010 CalNex campaign. *J. Geophys. Res.-Atmos.* 118(16):9233 – 9257.
28. Shepson PB, Mackay E, Muthuramu K (1996) Henry's law constants and removal processes for several atmospheric β-hydroxy alkyl nitrates. *Environ. Sci. Technol.* 30(12):3618–3623.
29. Rivera Rios JC (2018) Ph.D. thesis (Harvard University).
30. Bey I, et al. (2001) Global modeling of tropospheric chemistry with assimilated meteorology: Model description and evaluation. *J. Geophys. Res.-Atmos.* 106(D19):23073 – 23095.
31. Keller CA, et al. (2014) HEMCO v1. 0: A versatile, ESMF-compliant component for calculating emissions in atmospheric models. *Geosci. Model Dev.* 7(4):1409 – 1417.
32. Bates KH, Jacob DJ (2019) A new model mechanism for atmospheric oxidation of isoprene: Global effects on oxidants, nitrogen oxides, organic products, and secondary organic aerosol. *Atmos. Chem. Phys.* 19(14):9613 – 9640.

33. Fisher JA, et al. (2016) Organic nitrate chemistry and its implications for nitrogen budgets in an isoprene- and monoterpene-rich atmosphere: Constraints from aircraft (SEAC^{4}RS) and ground-based (SOAS) observations in the Southeast US. *Atmos. Chem. Phys.* 16(9):5969 – 5991.
34. Marais EA, et al. (2016) Aqueous-phase mechanism for secondary organic aerosol formation from isoprene: application to the southeast united states and co-benefit of SO_2 emission controls. *Atmos. Chem. Phys.* 16(3):1603 – 1618.
35. Browne EC, Wooldridge PJ, Min KE, Cohen RC (2014) On the role of monoterpene chemistry in the remote continental boundary layer. *Atmos. Chem. Phys.* 14(3):1225 – 1238.
36. Boyd CM, et al. (2015) Secondary organic aerosol formation from the β-pinene+NO_3 system: Effect of humidity and peroxy radical fate. *Atmos. Chem. Phys.* 15(13):7497 – 7522.
37. Pye HOT, et al. (2015) Modeling the current and future roles of particulate organic nitrates in the southeastern united states. *Environ. Sci. Technol.* 49(24):14195 – 14203.
38. Lee BH, et al. (2016) Highly functionalized organic nitrates in the southeast United States: Contribution to secondary organic aerosol and reactive nitrogen budgets. *P. Natl. Acad. Sci.* 113(6):1516 – 1521.